SUPPLEMENTARY MATERIALS FOR

S-functionalized Tripods with Monomethylene Spacers: Routes to Tetrairon(III) Single-molecule Magnets with Ultrashort Tethering Groups

Andrea Cornia [1,*], Chiara Danieli [1], Fabio Meglioli [1], Erik Tancini [1,2], Alessio Nicolini [1,2], Maria Jesus Rodriguez-Douton [1,#], Anne-Laure Barra [3], Marco Affronte [2] and Roberta Sessoli [4]

[1] *Department of Chemical and Geological Sciences, University of Modena and Reggio Emilia & INSTM, I-41125 Modena, Italy*

[2] *Department of Physics, Informatics, and Mathematics, University of Modena and Reggio Emilia, I-41125 Modena, Italy*

[3] *Laboratoire National des Champs Magnétiques Intenses-CNRS, Univ. Grenoble-Alpes, F-38042 Grenoble Cedex 9, France*

[4] *Department of Chemistry 'Ugo Schiff', University of Florence & INSTM, I-50019 Sesto Fiorentino (FI), Italy*

***** Correspondence: acornia@unimore.it; Tel.: +39-059-205-8645

\# Present address: NEST, Nanoscience Institute-CNR, I-56127 Pisa, Italy

Supplementary Note 1. Structure refinement details for **1**, **2**·Et_2O, **2**·0.375Et_2O and **3**.

[$Fe_4(L^{CH_2SCN})_2(dpm)_6$] (1). The well-developed, approximately isodiametric prisms of this compound are rhombohedral with a_{hex} = 16.95(2), c_{hex} = 56.10(8) Å at room temperature but monoclinic (space group *C*2/*c*) at 120 K. In the low-temperature structure, the Fe_4 units develop around crystallographic twofold axes parallel to *b* and the asymmetric unit therefore comprises half Fe_4 complex (*Z* = 4). One *t*Bu group is found resolvably disordered over two positions with 0.680(7) : 0.320(7) occupancies. All nonhydrogen atoms, including both components of the disordered *t*Bu group, were treated anisotropically.

[$Fe_4(L^{CH_2SAc})_2(dpm)_6$]·$Et_2O$ (2·Et_2O). Crystals grow as platelets belonging to triclinic space group $P\bar{1}$ and very prone to solvent loss. The asymmetric unit contains two Fe_4 molecules and two diethyl ether molecules (*Z* = 4). The first tetrairon(III) molecule (Fe1-Fe4, MOL1) shows major disorder effects on three *t*Bu groups, with occupancies 0.793(8) : 0.207(8), 0.751(7) : 0.249(7) and 0.848(6) : 0.152(6), respectively; both thioacetyl groups are ordered within experimental resolution. The second tetrairon(III) molecule (Fe5-Fe8, MOL2) also has three *t*Bu groups disordered over two positions with occupancies 0.779(6) : 0.221(6), 0.684(8) : 0.316(8) and 0.788(6) : 0.212(6), respectively. One of its thioacetyl groups is disordered over two positions with relative occupancies 0.591(3) : 0.409(3). The molecule of diethyl ether associated with MOL2 is also found disordered over two positions with relative occupancies 0.551(5) : 0.449(5). Non-hydrogen atoms were refined anisotropically, except for all minority components of disordered *t*Bu groups, for the C and O atoms of disordered thioacetyl group in MOL2, and for both components of disordered diethyl ether molecule.

[$Fe_4(L^{CH_2SAc})_2(dpm)_6$]·0.375$Et_2O$ (2·0.375Et_2O). This diethyl ether solvate forms apparently air-stable blocks which are triclinic, space group $P\bar{1}$. The asymmetric unit comprises two Fe_4 units and 0.75 diethyl ether molecules (*Z* = 4). The first tetrairon(III) molecule (Fe1-Fe4, MOL3) shows disorder only on three *t*Bu groups, which are split over two positions with occupancies 0.797(7) : 0.203(7), 0.633(5) : 0.367(5) and 0.671(10) : 0.329(10), respectively; both thioacetyl groups are ordered within experimental resolution. The second tetrairon(III) molecule (Fe5-Fe8, MOL4) contains two disordered *t*Bu groups, with occupancies 0.525(5) : 0.475(5) and 0.706(7) : 0.294(7). One thioacetyl groups is split over two positions with occupancies 0.6866(15) (S3Ac) and 0.3134(15) (S4Ac). The second thioacetyl group is disordered over three positions, namely S5Ac, S6Ac and S7Ac, with occupancies 0.4366(15), 0.3134(15) and 0.2500. The reported site occupancies have been refined so as to be structurally compatible with the occurrence of a disordered diethyl ether molecule, which was clearly located in two distinct positions. The first position has realistic contacts with S5Ac but not with the other components of the disordered thioacetyl. Hence, its occupancy was constrained to be the same as that of S5Ac. The second diethyl ether component gives realistic contacts with both S5Ac and S6Ac, but not with S7Ac. However, its contacts with S3Ac/S4Ac of a neighbouring molecule are realistic only for S4Ac. Its occupancy was then constrained to be the same as that of S4Ac. In the final stages of refinement, the combined occupancy of diethyl ether molecules converged to ca. 0.74 and was then constrained to 0.7500 for simplicity. Nonhydrogen atoms were treated anisotropically, except for disordered carbon atoms of *t*Bu groups

with occupancy less than 2/3, and for C and O atoms of minority thioacetyl components and of solvent molecules.

[$Fe_4(L^{CH_2SS\textit{n}Bu})_2(dpm)_6$] (3). Crystals of this unsolvated phase grow as very fragile red prisms belonging to monoclinic space group *C*2/*c*. Fe_4 units develop around crystallographic twofold axes parallel to *b* and the asymmetric unit therefore comprises half Fe_4 complex ($Z = 4$). One *t*Bu group is found resolvably disordered over two positions with 0.764(8) : 0.236(8) occupancies. The side chain of the tripodal ligand is split over at least three positions, as clearly shown by the electron density peaks of S atoms. However, location of the *n*Bu group proved extremely challenging. The final model converged reasonably well with 0.801(2) : 0.0794(17) : 0.120(2) occupancies and enhanced rigid-body restraints (RIGU) [1] on the anisotropic displacement parameters of the major component. Nonhydrogen atoms were treated anisotropically, except for minority components of disordered moieties.

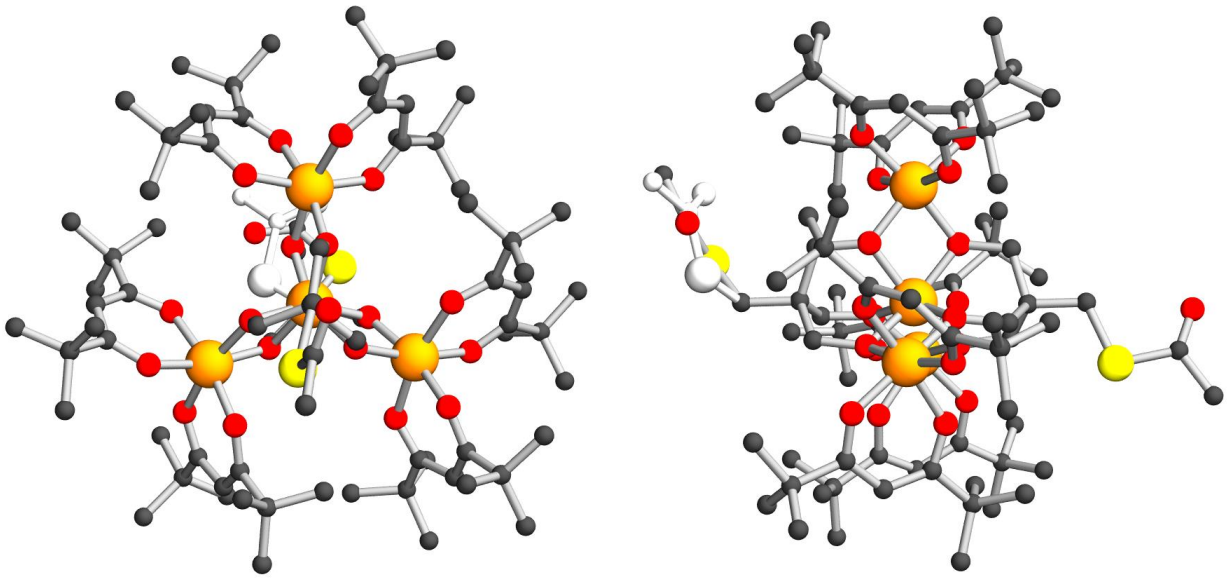

(**a**) (**b**)

Figure S1. Molecular structure of MOL2 in **2**·Et_2O viewed along (**a**) and perpendicular to (**b**) the idealized threefold axis. Same color code as in Figure 1. The minority component of disordered thioacetyl group is shown in light gray. Minority components of disordered *t*Bu groups and hydrogen atoms have been omitted.

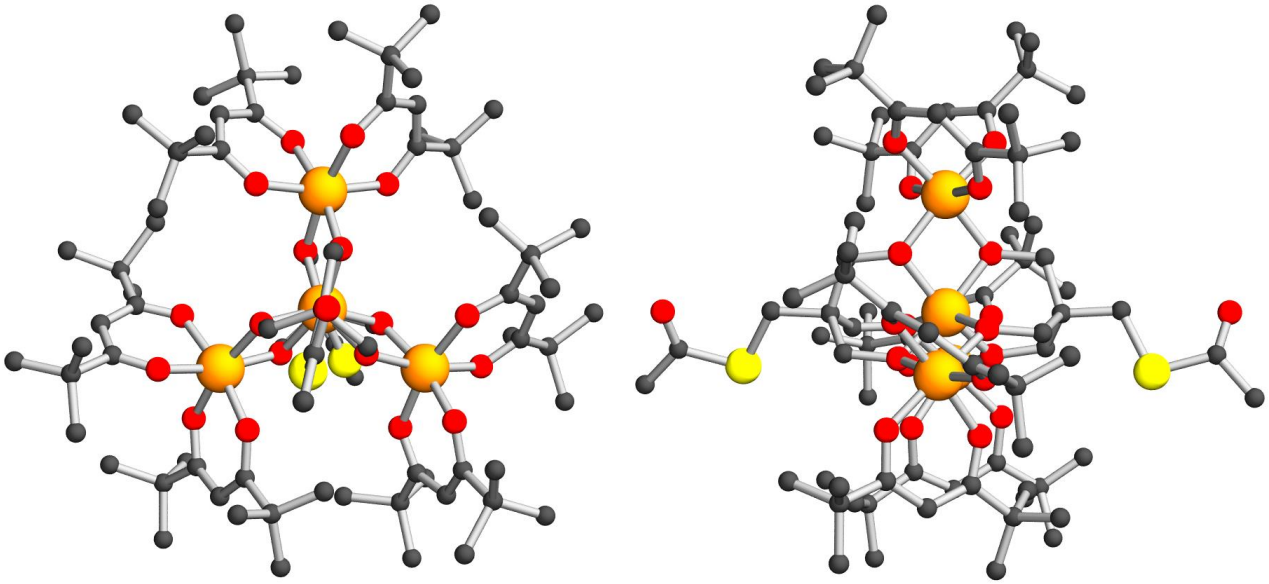

(**a**) (**b**)

Figure S2. Molecular structure of MOL3 in **2**·0.375Et_2O viewed along (**a**) and perpendicular to (**b**) the idealized threefold axis. Same color code as in Figure 1. Minority components of disordered *t*Bu groups and hydrogen atoms have been omitted.

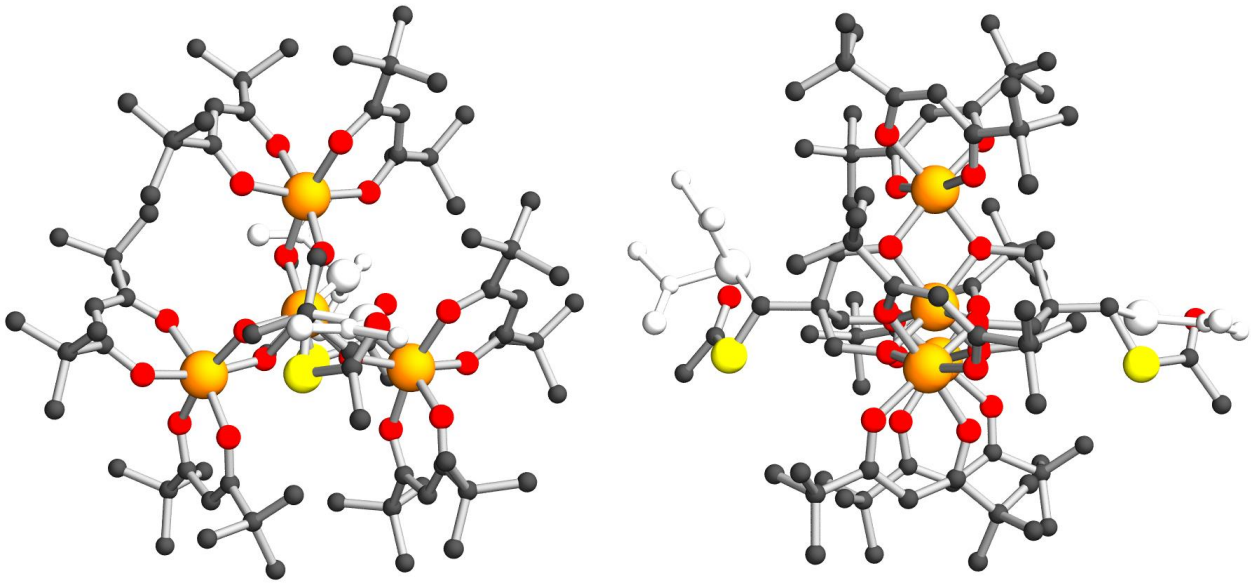

(**a**) (**b**)

Figure S3. Molecular structure of MOL4 in **2**·0.375Et_2O viewed along (**a**) and perpendicular to (**b**) the idealized threefold axis. Same color code as in Figure 1. The minority components of disordered thioacetyl groups are shown in light gray. Minority components of disordered *t*Bu groups and hydrogen atoms have been omitted.

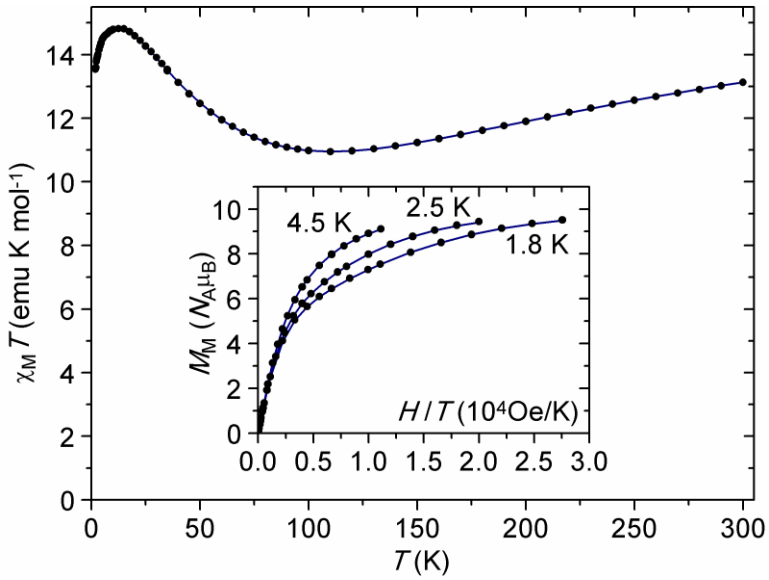

Figure S4. Temperature dependence of the molar magnetic susceptibility in low field, and molar magnetization isotherms at low temperature (inset) for **2**·Et_2O. Solid lines represent the best-fit curves.

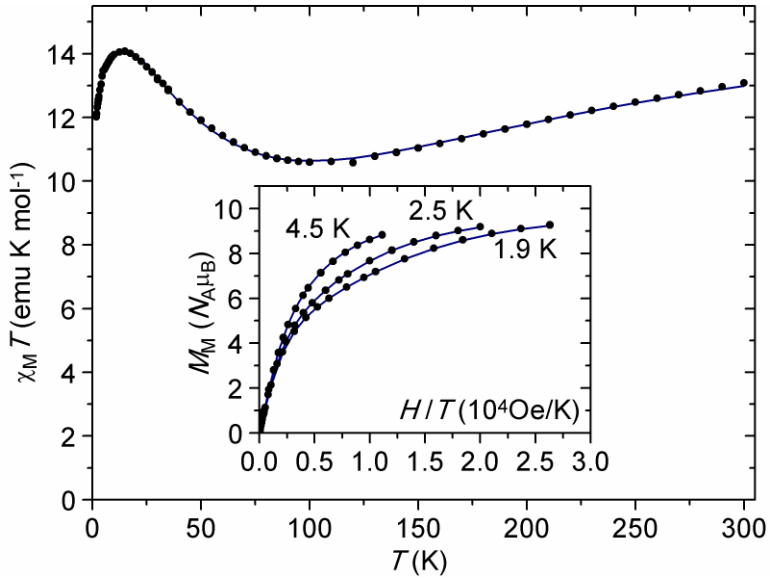

Figure S5. Temperature dependence of the molar magnetic susceptibility in low field, and molar magnetization isotherms at low temperature (inset) for **3**. Solid lines represent the best-fit curves.

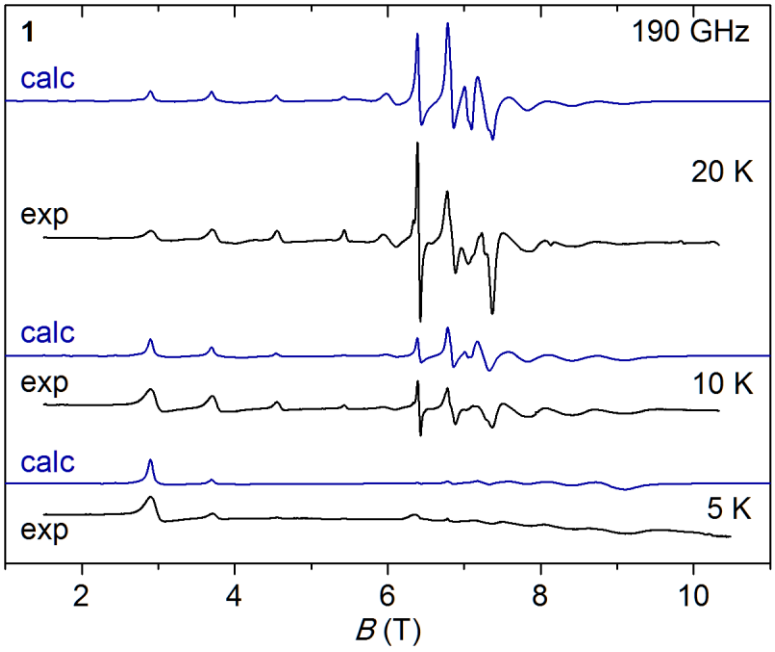

Figure S6. Temperature dependent HF-EPR spectra of **1** at 190 GHz (black traces) along with best simulations (blue traces).

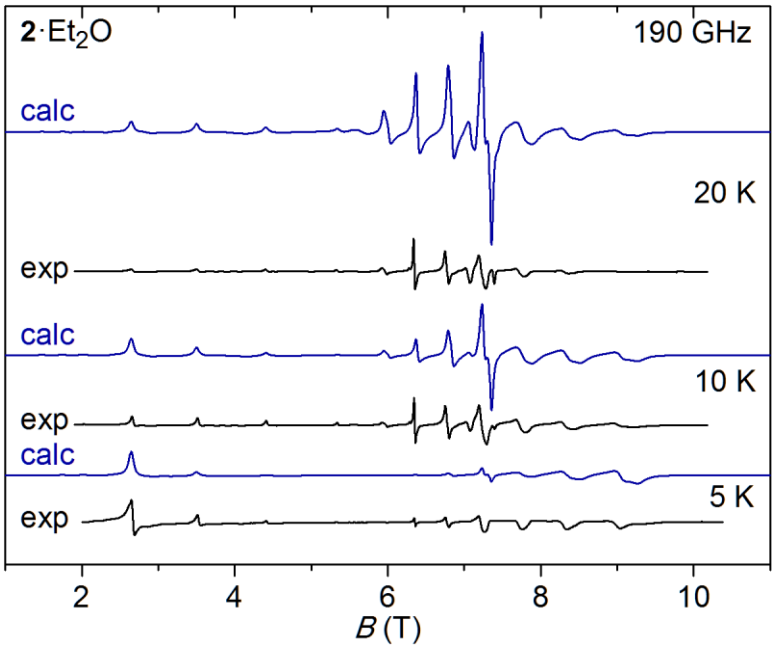

Figure S7. Temperature dependent HF-EPR spectra of **2**·Et_2O at 190 GHz (black traces) along with best simulations (blue traces).

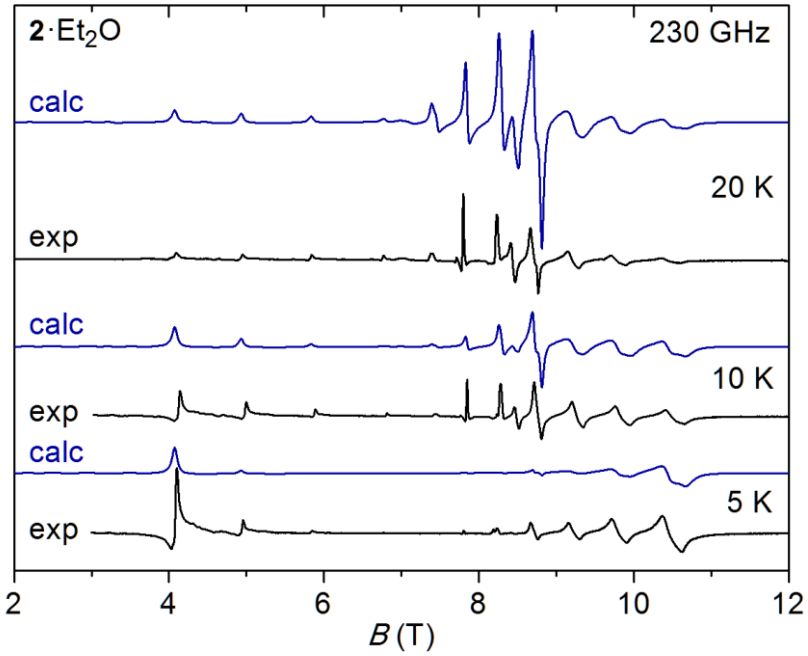

Figure S8. Temperature dependent HF-EPR spectra of **2**·Et_2O at 230 GHz (black traces) along with best simulations (blue traces).

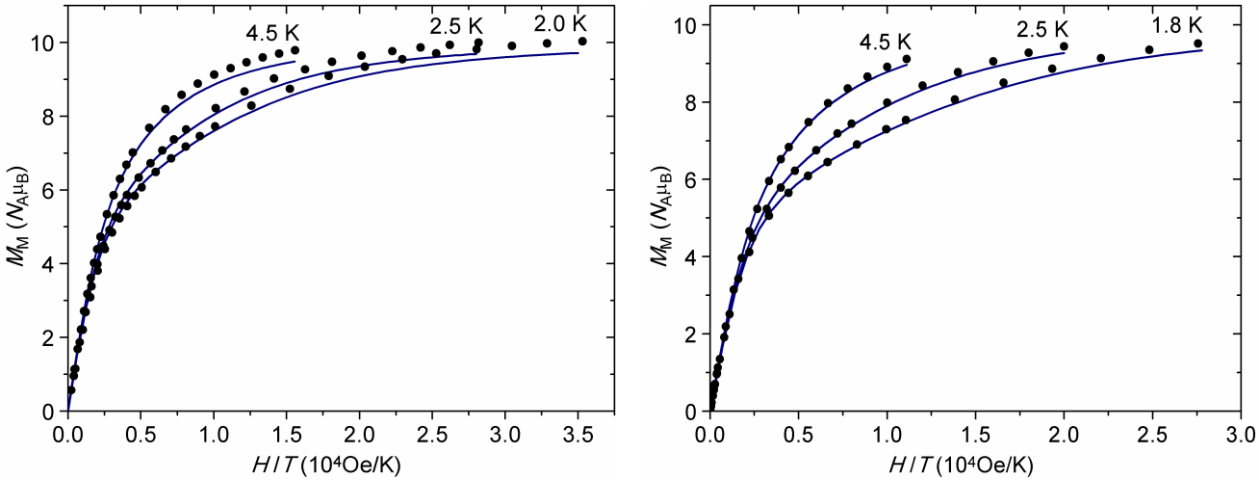

(**a**) (**b**)

Figure S9. Molar magnetization isotherms recorded on **1** (**a**) and **2**·Et_2O (**b**) compared with calculated curves (PHI v3.1.5 [2]) based on HF-EPR parameters in Table 1.

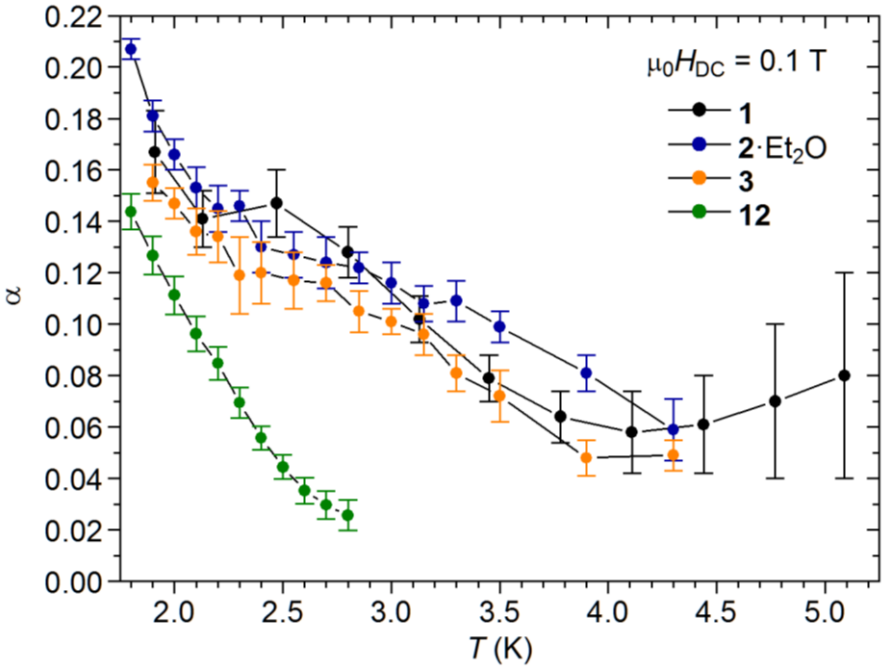

Figure S10. Temperature dependence of the α parameter in a 0.1 T applied static field for **1**, **2**·Et_2O, **3** and **12** [3].

Table S1. Crystal data and refinement parameters for **1**, **2**·Et_2O, **2**·0.375Et_2O and **3**.

	1	**2**·Et_2O	**2**·0.375Et_2O	**3**
Formula	$C_{78}H_{130}Fe_4N_2O_{18}S_2$	$C_{84}H_{146}Fe_4O_{21}S_2$	$C_{81.50}H_{139.75}Fe_4O_{20.38}S_2$	$C_{84}H_{148}Fe_4O_{18}S_4$
Formula weight	1671.35	1779.53	1733.20	1797.66
T (K)	120(2)	120(2)	140(2)	140(2)
λ (Å)	0.71073	0.71073	0.71073	0.71073
Crystal size (mm^3)	0.60×0.45×0.35	0.52×0.51×0.24	0.63×0.51×0.39	0.57×0.47×0.16
Crystal system	monoclinic	triclinic	triclinic	monoclinic
Space group	*C*2/*c* (No. 15)	$P\bar{1}$ (No. 2)	$P\bar{1}$ (No. 2)	*C*2/*c* (No. 15)
a (Å)	27.8089(12)	15.9287(6)	15.8696(4)	19.5646(5)
b (Å)	17.3432(8)	24.8996(11)	19.5070(5)	22.6693(5)
c (Å)	20.7771(8)	26.7398(12)	32.5981(8)	25.1428(6)
α (°)	90.00	68.529(2)	97.1881(12)	90
β (°)	117.3181(14)	77.634(2)	102.1501(12)	116.6093(9)
γ (°)	90.00	81.590(2)	104.3036(13)	90
V ($Å^3$)	8903.1(7)	9613.6(7)	9390.9(4)	9970.1(4)
Z	4	4	4	4
D_{calcd} (g cm^{-3})	1.247	1.229	1.226	1.198
μ(MoK_α) (mm^{-1})	0.747	0.697	0.712	0.711
F(000)	3568	3816	3711	3856
θ range (°)	3.30-28.04	1.67-26.18	1.95-27.01	2.01-26.02
Reflns collected	47022	167802	138502	62516
R_{int}	0.0302	0.0400	0.0296	0.0272
Data/restraints/parameters	10747/42/501	38056/50/2054	39675/365/2008	9810/86/555
Goodness-of-fit on F^2	1.069	1.012	1.040	1.058
Final R indices [I>2σ(I)]	R1 = 0.0438, wR2 = 0.1235	R1 = 0.0505, wR2 = 0.1247	R1 = 0.0602, wR2 = 0.1442	R1 = 0.0565, wR2 = 0.1731
R indices (all data)	R1 = 0.0644, wR2 = 0.1352	R1 = 0.0841, wR2 = 0.1455	R1 = 0.0994, wR2 = 0.1754	R1 = 0.0722, wR2 = 0.1855
Largest diff. peak/hole ($eÅ^{-3}$)	0.847/–0.381	2.230/–0.731	1.130/–1.241	1.334/–0.870

Table S2. Geometrical parameters for the coordination sphere of the central iron ion in **1**, **2**·Et_2O, **2**·0.375Et_2O, **3** and **12**, after averaging according to D_3 symmetry [4].

Compound	α (°)	β (°)	γ (°)	θ (°)	ϕ (°)
1	88.88	77.43	70.17	53.95	30.38
2·Et_2O (MOL1, MOL2)	89.34, 89.37	77.62, 77.14	68.70, 69.41	54.27, 54.29	32.58, 31.32
2·0.375Et_2O (MOL3, MOL4)	89.30, 89.67	77.63, 77.17	68.78, 68.60	54.25, 54.50	32.48, 32.46
3	89.23	77.98	68.40	54.20	33.19
12 [a]	89.24	77.20	69.65	54.20	31.04

[a] Ref. [3]

Table S3. Linewidths (in Gauss) used to simulate HF-EPR spectra for compounds **1**, **2**·Et_2O, and **12**, depending on the transition ($M \rightarrow M'$) and on magnetic field orientation (x, y or z).[a]

Compound	−5 → −4, −4 → −3			−3 → −2			−2 → −1			−1 → 0			|ΔM| > 1		
	x	*y*	*z*	*x*	*y*	*z*	*x*	*y*	*z*	*x*	*y*	*z*	*x*	*y*	*z*
1	1800	1800	400	1400	1400	400	800	800	400	300	300	300	1800	1800	1800
2·Et_2O	800	1100	400	800	1100	400	300	300	400	300	300	400	1800	1800	1800
12	800	600	400	800	600	400	400	400	400	400	400	400	1800	1800	1800

[a] For the same compound, the same linewidths were used at all frequencies and temperatures; transitions $-M' \rightarrow -M$ were assigned the same linewidths as $M \rightarrow M'$.

Table S4. Fitting parameters of the isothermal χ_M'' vs. ν curves (H_{DC} = 1 kOe) based on the extended Debye model for compound **1**.

T (K)	$\chi_{M,T} - \chi_{M,S}$ (emu mol^{-1})	τ (μs)	α
1.91	5.60(11)	618(17)	0.167(16)
2.13	4.96(7)	295(6)	0.141(11)
2.47	4.40(7)	111(3)	0.147(13)
2.80	3.76(5)	54.1(10)	0.128(10)
3.13	3.16(4)	31.4(6)	0.102(9)
3.45	2.65(4)	20.5(5)	0.079(9)
3.78	2.24(5)	14.5(5)	0.064(10)
4.11	1.91(9)	10.8(8)	0.058(16)
4.44	1.65(13)	8.3(9)	0.061(19)
4.77	1.4(2)	6.6(16)	0.07(3)
5.09	1.2(3)	5.6(18)	0.08(4)

Table S5. Fitting parameters of the isothermal χ_M'' vs. ν curves (H_{DC} = 1 kOe) based on the extended Debye model for compound **2**·Et_2O.

T (K)	$\chi_{M,T} - \chi_{M,S}$ (emu mol^{-1})	τ (μs)	α
1.80	6.36(4)	4160(40)	0.207(4)
1.90	5.91(4)	2550(30)	0.181(6)
2.00	5.59(4)	1680(20)	0.166(6)
2.10	5.28(5)	1150(20)	0.153(8)
2.20	5.04(5)	821(14)	0.145(9)
2.30	4.84(3)	605(7)	0.146(6)
2.40	4.58(6)	448(9)	0.130(10)
2.40	4.57(5)	443(9)	0.130(10)
2.55	4.30(4)	299(5)	0.127(9)
2.70	4.04(5)	209(4)	0.124(10)
2.85	3.80(3)	151.7(18)	0.122(6)
3.00	3.56(4)	112.5(17)	0.116(8)
3.15	3.34(3)	85.6(11)	0.108(7)
3.30	3.16(3)	67.4(10)	0.109(8)
3.50	2.91(2)	50.6(5)	0.099(6)
3.90	2.46(2)	31.2(4)	0.081(7)
4.30	2.05(4)	21.9(6)	0.059(12)

Table S6. Fitting parameters of the isothermal χ_M'' vs. ν curves (H_{DC} = 1 kOe) based on the extended Debye model for compound **3**.

T (K)	$\chi_{M,T} - \chi_{M,S}$ (emu mol^{-1})	τ (μs)	α
1.90	4.57(4)	1730(30)	0.155(7)
2.00	4.37(3)	1173(14)	0.147(6)
2.10	4.13(5)	807(15)	0.136(9)
2.20	3.96(5)	590(12)	0.134(10)
2.30	3.77(7)	430(13)	0.119(15)
2.40	3.60(5)	323(7)	0.120(12)
2.55	3.38(5)	218(5)	0.117(11)
2.70	3.20(3)	154(2)	0.116(7)
2.85	2.98(3)	110.4(16)	0.105(8)
3.00	2.801(17)	82.6(8)	0.101(5)
3.15	2.64(3)	62.6(9)	0.096(8)
3.30	2.45(2)	49.2(6)	0.081(7)
3.50	2.27(3)	36.7(6)	0.072(10)
3.90	1.896(18)	22.7(3)	0.048(7)
4.30	1.625(18)	15.0(2)	0.049(6)

References

1. Thorn, A.; Dittrich, B.; Sheldrick, G.M. Enhanced rigid-bond restraints. *Acta Crystallogr. Sect. A Found. Crystallogr.* **2012**, *68*, 448–451, doi:10.1107/S0108767312014535.
2. Chilton, N. F.; Anderson, R. P.; Turner, L. D.; Soncini, A.; Murray, K. S. PHI: A Powerful New Program for the Analysis of Anisotropic Monomeric and Exchange-Coupled Polynuclear d- and f-Block Complexes. *J. Comput. Chem.* **2013**, *34*, 1164−1175.
3. Serrano, G.; Poggini, L.; Briganti, M.; Sorrentino, A.L.; Cucinotta, G.; Malavolti, L.; Cortigiani, B.; Otero, E.; Sainctavit, P.; Loth, S.; et al. Quantum dynamics of a single molecule magnet on superconducting Pb(111). *Nat. Mater.* **2020**, *19*, 546–551, doi:10.1038/s41563-020-0608-9.
4. Gregoli, L.; Danieli, C.; Barra, A.-L.; Neugebauer, P.; Pellegrino, G.; Poneti, G.; Sessoli, R.; Cornia, A. Magnetostructural correlations in tetrairon(III) single-molecule magnets. *Chem. Eur. J.* **2009**, *15*, 6456–6467, doi:10.1002/chem.200900483.